

Coarse Master Equations for Peptide Folding Dynamics[†]

Nicolae-Viorel Buchete[‡] and Gerhard Hummer^{*}

Laboratory of Chemical Physics, National Institute of Diabetes and Digestive and Kidney Diseases,
National Institutes of Health, Bethesda, Maryland 20892-0520

Received: August 2, 2007; In Final Form: October 25, 2007

We construct coarse master equations for peptide folding dynamics from atomistic molecular dynamics simulations. A maximum-likelihood propagator-based method allows us to extract accurate rates for the transitions between the different conformational states of the small helix-forming peptide Ala5. Assigning the conformational states by using transition paths instead of instantaneous molecular coordinates suppresses the effects of fast non-Markovian dynamics. The resulting master equations are validated by comparing their analytical correlation functions with those obtained directly from the molecular dynamics simulations. We find that the master equations properly capture the character and relaxation times of the entire spectrum of conformational relaxation processes. By using the eigenvectors of the transition rate matrix, we are able to systematically coarse-grain the system. We find that a two-state description, with a folded and an unfolded state, roughly captures the slow conformational dynamics. A four-state model, with two folded and two unfolded states, accurately recovers the three slowest relaxation process with time scales between 1.5 and 7 ns. The master equation models not only give access to the slow conformational dynamics but also shed light on the molecular mechanisms of the helix–coil transition.

1. Introduction

Molecular dynamics (MD) simulations provide a unique tool to explore the structure, energetics, and dynamics of biomolecules. Broad spatial and temporal scales are accessible, ranging from atomic motions on quantum energy surfaces to protein binding and association in macromolecular assemblies. Across the different time and length scales, MD simulations offer an exhaustively detailed description of the motion of every atom and the resulting thermodynamic and kinetic properties.¹

However, the great temporal and spatial resolution of MD comes at a price: time scale limitations and potentially overwhelming detail. On one hand, the characteristic times of many biologically relevant processes remain out of reach. Despite enormous progress in accelerating the simulations, the ~ 1 -fs time step used in the integration of the equations of motion is set firmly by fast time scales of molecular vibrations and collisions, requiring $\sim 10^{15}$ integration steps to reach the seconds time scale, well beyond the reach of current technology. On the other hand, the level of detail contained in a simulation trajectory, with the path of every single protein atom or water molecule traced out in space, can be overwhelming. As a result, the interpretation of simulation data for complex molecular systems itself requires increasingly sophisticated analysis methodologies.

Master equations^{2–10} provide a powerful framework within which both challenges can be addressed. By describing the system at a coarser level, master equations enable analytical treatments and thereby address the time scale problem; at the same time, they focus from the onset on the dynamics of the

most relevant aspects of the system, thus aiding in the subsequent analysis.

The formal development of master equations is well-rooted in statistical mechanics and closely connected to the projection–operator formalism.¹¹ In essence, the motions of the detailed molecular system are projected onto a discrete representation of the conformation space, and equations of motion for this projection are developed. The functions to be projected on typically have finite support, defining cells in conformation space. For proteins, one can, for instance, use the number of “correct bonds” or native amino acid conformations,^{12,13} dihedral angles, or amino acid contacts. The master equation then describes the dynamics of the populations in each of the respective states.

Master equations can be exact representations of the system; for instance, of lattice models in protein folding.¹⁴ Here, we are concerned with systems in which they provide, at best, good approximations. With the implicit assumption of Markovian (i.e., memoryless) dynamics, the resulting approximate master equations can be cast in the form of kinetic rate equations (see eqs 1 and 2, below). However, other representations are possible. For instance, the Fokker–Planck equation for diffusion discretized in space also takes on the form of a master equation.¹⁵ Accurate diffusion models can thus be obtained from simulation trajectories by first fitting a master equation.^{16,17}

MD simulations provide a means to construct approximate master equations that accurately incorporate detailed molecular information. By projecting the simulation trajectories onto the states of the master equation model, one can effectively parametrize the equations of motion in the coarse space. Similar projection procedures have been used in coarse molecular dynamics.¹⁸

A common assumption is that the dynamics within the space of coarse coordinates is, indeed, Markovian. Clearly, this is not likely the case in practice. Unless one uses a very large coarse

[†] Part of the “Attila Szabo Festschrift”.

^{*} To whom correspondence should be addressed. Email: gerhard.hummer@nih.gov.

[‡] Current address: School of Physics, University College Dublin, Belfield, Dublin 4, Ireland.

space that includes coordinates not only for the solute (here, a protein) but also the solvent,^{19,20} the neglected degrees of freedom will not simply average out but lead to non-Markovian dynamics, at least at short times.

Finding optimal methods to partition the conformation space of a biomolecule into discrete states remains a central problem in building coarse models.^{4,5,21–29} A number of methods have been developed for this purpose,^{30–32} but the challenge remains to avoid arbitrary decisions in state assignments and to develop fully automated and unbiased state partitioning algorithms.³³ In this work, we are not concerned with identifying optimal coarse states of a molecular system. Instead, we explore if one can construct useful master equations given an assignment in which states are reasonably well identified, but not well enough that the dynamics is truly Markovian.

The focus here is on three main aspects: how can one construct master equation models that accurately capture the dynamics over a broad range of time scales? How sensitive are the resulting models to details in their construction, in particular, the assignment of conformations to coarse states? And how can one analyze the resulting master equation models to extract useful minimal descriptions of the molecular motions?

The paper is organized as follows. We will first introduce relevant aspects of the master equation formalism, including analytic expressions for propagators and correlation functions. We will then describe methods to construct master equations from simulation data. To illustrate and test this formalism, we will study the helix–coil transition of a blocked Ala5 pentapeptide in water. Short polyalanine peptides have been studied extensively using both experimental and theoretical methods.^{34–47} Ala5 is small enough to permit an exhaustive investigation with MD simulations. Nevertheless, it is complex enough to require $2^5 = 32$ conformational states, even if one uses only “helix” and “coil” designations for each of the five amino acids. To construct master equations for the populations of the 32 states, we perform MD simulations of Ala5 in water covering 1 μ s each at 250, 300, and 400 K. To assign the conformational states, we will use two different methods: one using instantaneous dihedral angles and the other transition paths. From the resulting trajectories in the space of the 32 states, we will construct master equations first using lifetimes and branching probabilities and then using a maximum likelihood propagator-based (MLPB) method that better suppresses the problems arising from fast non-Markovian dynamics. The validity of the resulting master equations will be assessed by comparing correlation functions from actual simulation trajectories with the analytical predictions of the master equation models. By analyzing the eigenstates of the master equation models, we show that the slow conformational dynamics can be described roughly by using two states (folded/helix and unfolded/coil), and accurately by using four states. This additional coarse-graining allows us to explore the mechanisms of the helix–coil transition in the Ala5 system.

2. Theory

2.1. Master Equation. To construct a master equation for the equilibrium conformational dynamics of the peptide, we follow the approach of ref 10. We divide the peptide configuration space into N non-overlapping cells. As shown by Zwanzig,¹¹ the populations in the cells evolve according to a generalized, integro-differential master equation. If the dynamics of the populations is non-Markovian but with rapidly decaying memory, we can describe the time evolution accurately in terms of a simple master equation,

$$\dot{P}_i(t) = \sum_{j=1}^N [k_{ij}P_j(t) - k_{ji}P_i(t)] \quad (1)$$

where $P_i(t)$ is the population of state i , $k_{ji} \geq 0$ is the rate of transitions from state i to state j , and $\dot{P}_i \equiv dP_i/dt$. In vector–matrix notation, eq 1 becomes

$$\dot{\mathbf{P}}(t) = \mathbf{K}\mathbf{P}(t) \quad (2)$$

where the $N \times N$ rate matrix \mathbf{K} has off-diagonal elements $k_{ji} \geq 0$ and diagonal elements $k_{ii} = -\sum_{j \neq i} k_{ji} < 0$. For a connected state space, we have a unique, stationary equilibrium distribution,

$$\mathbf{K}\mathbf{P}_{\text{eq}} \equiv 0 \quad (3)$$

that we assume to be nonzero and normalized, $P_{\text{eq}}(i) > 0$ and $\sum_{i=1}^N P_{\text{eq}}(i) = 1$. By invoking the condition of detailed balance,

$$k_{ij}P_{\text{eq}}(j) = k_{ji}P_{\text{eq}}(i) \quad (4)$$

we define the elements of the symmetrized rate matrix as

$$k_{ij}^{\text{sym}} = P_{\text{eq}}^{-1/2}(i) k_{ij} P_{\text{eq}}^{1/2}(j) = (k_{ij}k_{ji})^{1/2} \quad (5)$$

or in matrix notation,

$$\mathbf{K}^{\text{sym}} = \mathbf{P}_{\text{eq}}^{-1/2} \mathbf{K} \mathbf{P}_{\text{eq}}^{1/2} \quad (6)$$

with $\mathbf{P}_{\text{eq}} = \text{diag}[P_{\text{eq}}(1), P_{\text{eq}}(2), \dots, P_{\text{eq}}(N)]$.

2.2. Eigenvalues and Eigenvectors. The symmetrized rate matrix \mathbf{K}^{sym} has eigenvalues λ_n with corresponding orthonormal eigenvectors ϕ_n given by

$$\mathbf{K}^{\text{sym}}\phi_n = \lambda_n\phi_n \quad (7)$$

One of the eigenvalues is zero, and all others are real and negative. In the following, we assume that the eigenvalues are sorted by magnitude: $\lambda_1 = 0 > \lambda_2 \geq \lambda_3 \geq \dots \geq \lambda_N$. The λ_n are also the eigenvalues of the original, nonsymmetric rate matrix, with corresponding left and right eigenvectors ψ_n^{L} and ψ_n^{R} , respectively, that satisfy

$$\begin{aligned} \mathbf{K}\psi_n^{\text{R}} &= \lambda_n\psi_n^{\text{R}} \\ \psi_n^{\text{L}}\mathbf{K} &= \lambda_n\psi_n^{\text{L}} \end{aligned} \quad (8)$$

The i th elements of the left and right eigenvectors are related to the corresponding elements of the eigenvectors of the symmetrized rate matrix through

$$\begin{aligned} \psi_n^{\text{L}}(i) &= P_{\text{eq}}^{-1/2}(i) \phi_n(i) \\ \psi_n^{\text{R}}(i) &= P_{\text{eq}}^{1/2}(i) \phi_n(i) \end{aligned} \quad (9)$$

It follows from eq 3 that the first right eigenvector (for eigenvalue $\lambda_1 = 0$) of \mathbf{K} is given by the equilibrium population, $\psi_1^{\text{R}}(i) = P_{\text{eq}}(i)$. From eq 9, one then finds that $\phi_1(i) = P_{\text{eq}}^{1/2}(i)$ and $\psi_1^{\text{L}}(i) = 1$. From the orthonormality of the ϕ_n , one obtains the normalization conditions

$$\begin{aligned} \sum_{i=1}^N \psi_n^L(i) \psi_m^L(i) P_{\text{eq}}(i) &= \sum_{i=1}^N \psi_n^R(i) \psi_m^R(i) / P_{\text{eq}}(i) \\ &= \sum_{i=1}^N \psi_n^R(i) \psi_m^L(i) = \sum_{i=1}^N \phi_n(i) \phi_m(i) = \delta_{nm} \quad (10) \end{aligned}$$

where δ_{nm} is the Kronecker delta. It follows that $\sum_{i=1}^N \psi_n^R(i) = \sum_{i=1}^N P_{\text{eq}}(i) \psi_n^L(i) = \delta_{1n}$.

2.3. Propagators and Correlation Functions. The solution to the master eq 2 in terms of a matrix exponential is

$$\mathbf{P}(t) = \exp(\mathbf{K}t)\mathbf{P}(0) \quad (11)$$

By using the spectral decomposition, we can express the time-dependent populations as

$$\mathbf{P}(t) = \sum_{n=1}^N \psi_n^R[\psi_n^L \cdot \mathbf{P}(0)] e^{\lambda_n t} \quad (12)$$

The projection of the initial state $\mathbf{P}(0)$ onto each of the left-hand eigenvectors ψ_n^L thus determines the amplitude of the corresponding exponential phases with relaxation time $\tau_n = -1/\lambda_n$. The right-hand eigenvectors give the weight of the phase for each of the states. It follows that the propagators (or Green's function), defined as the probability of being in state j at time t , given that the system was in state i at time 0, can be written as

$$p(j, t|i, 0) = [e^{\mathbf{K}t}]_{ji} = \sum_{n=1}^N \psi_n^R(j) \psi_n^L(i) e^{\lambda_n t} \quad (13)$$

The rate matrix \mathbf{K} is therefore the generator of the dynamics, and its matrix exponential defines a transition matrix for time t . Indeed, rather than using \mathbf{K} itself, we could use the transition matrix $\exp(\mathbf{K}t)$ to propagate the system over discrete time intervals t .

Following the formalism of Bicout and Szabo,¹⁵ we express correlation functions in terms of eigenmodes. Specifically, we use eq 13 to calculate correlation functions in state space. If $s(t) \in \{1, 2, \dots, N\}$ is the state of the system at time t , and \mathbf{f} and \mathbf{g} are vectors with elements $f[i]$ and $g[i]$, respectively, then the correlation function $\langle g[s(t)] f[s(0)] \rangle$ can be written as

$$\begin{aligned} \tilde{c}(t) &= \langle g[s(t)] f[s(0)] \rangle = \lim_{T \rightarrow \infty} T^{-1} \int_0^T g[s(\tau + t)] f[s(\tau)] d\tau \\ &= \sum_{i,j=1}^N g[j] f[i] p(j, t|i, 0) P_{\text{eq}}(i) = \sum_{n=1}^N e^{\lambda_n t} (\mathbf{g} \cdot \psi_n^R)(\mathbf{f} \cdot \psi_n^R) \quad (14) \end{aligned}$$

The corresponding normalized correlation function $c(t) = [\tilde{c}(t) - \tilde{c}(\infty)] / [\tilde{c}(0) - \tilde{c}(\infty)]$ becomes

$$c(t) = \frac{\sum_{n=2}^N e^{\lambda_n t} (\mathbf{g} \cdot \psi_n^R)(\mathbf{f} \cdot \psi_n^R)}{\sum_{n=2}^N (\mathbf{g} \cdot \psi_n^R)(\mathbf{f} \cdot \psi_n^R)} \quad (15)$$

where we used that $\lambda_1 = 0$. If we project the trajectory in state space onto the left-hand eigenvectors, $\mathbf{f} = \psi_m^L$ and $\mathbf{g} = \psi_l^L$ and use their normalization eq 10, we obtain single-exponential decays (without explicit normalization!):

$$\tilde{c}_{lm}(t) = \langle \psi_m^L[s(t)] \psi_l^L[s(0)] \rangle = \delta_{lm} e^{\lambda_m t} \quad (16)$$

with amplitude 1 if $m = l$ and 0 if $m \neq l$. Note that for $n > 1$ the normalized and unnormalized auto-correlation functions are identical: $C_{nn}(t) = [\tilde{C}_{nn}(t) - \tilde{C}_{nn}(\infty)] / [\tilde{C}_{nn}(0) - \tilde{C}_{nn}(\infty)] = \tilde{C}_{nn}(t)$. Later, we will use eq 16 to validate the fitted master equation against actual simulation trajectories.

2.4. Coarse Graining of the Master Equation. In many practical cases, the number of states, N , will be large, and one would like to reduce that number to M states by grouping the N states into $M < N$ nonoverlapping classes. Such clustering will be particularly useful if a gap exists in the sorted eigenvalue spectrum beyond eigenvalue M ; that is, $\lambda_2 \approx \lambda_3 \approx \dots \approx \lambda_M \gg \lambda_{M+1}$.

The spectral decompositions of the time-dependent populations and state-space correlation functions, eqs 11 and 14, are suggestive with respect to such further coarse graining. A grouping corresponds to finding a set of vectors \mathbf{v}_m with elements $v_m(i) = 0$ or 1 and $\sum_{m=1}^M v_m(i) = 1$ that provide the support for class m [i.e., if $v_m(i) = 1$, then state i belongs to class m]. The unnormalized number correlation function for being in class m is then $\tilde{c}_m(t) = \langle v_m[s(t)] v_m[s(0)] \rangle$. The corresponding normalized correlation function is $c_m(t) = [\tilde{c}_m(t) - \tilde{c}_m(\infty)] / [\tilde{c}_m(0) - \tilde{c}_m(\infty)]$. Following Bicout and Szabo,⁴⁸ one can search for the grouping that makes the normalized number correlation function as single-exponential as possible for the slowest relaxation time. By using eq 14, the normalized number correlation function for class m becomes

$$\begin{aligned} c_m(t) &= \frac{\sum_{n=2}^N e^{\lambda_n t} (\mathbf{v}_m \cdot \psi_n^R)^2}{\sum_{n=2}^N (\mathbf{v}_m \cdot \psi_n^R)^2} \\ &= \frac{\sum_{n=2}^N e^{\lambda_n t} (\mathbf{v}_m \cdot \psi_n^R)^2}{f(1-f)} \quad (17) \end{aligned}$$

where $f = \mathbf{v}_m \cdot \mathbf{P}_{\text{eq}}$ is the equilibrium population of class m . The "best" two-state representation can then be found by maximizing the amplitude of the slowest relaxation, λ_2 (note: $\lambda_1 = 0$), over the elements of the projection, $v_m(i) \in \{0, 1\}$:

$$\max_{v_m(i) \in \{0,1\}} \frac{(\mathbf{v}_m \cdot \psi_2^R)^2}{\mathbf{v}_m \cdot \mathbf{P}_{\text{eq}} (1 - \mathbf{v}_m \cdot \mathbf{P}_{\text{eq}})} \quad (18)$$

For continuous $v_m(i)$, the maximum would be $v_m(i) = \psi_2^L(i)$, which according to eq 16 would give a single exponential with the optimal amplitude of 1. For the discrete $v_m(i)$, ignoring the denominator, a large amplitude will be obtained if the sign is retained, $v_m(i) = 1$ for $\psi_2^L(i) > 0$, and $v_m(i) = 0$ for $\psi_2^L(i) \leq 0$. [We note that $\psi_n^R(i)$ and $\psi_n^L(i)$ have the same sign, as follows from eq 9.]

To cluster the system into three states, one would maximize the amplitudes for the slowest two relaxation processes corresponding to eigenvalues λ_2 and λ_3 . Following arguments as in the two-state case, using signs of the eigenvectors leads to an approximate solution. After the appropriate sign change, $\psi_2^L(i)$ and $\psi_3^L(i)$ are both positive, negative and positive, or positive and negative, respectively. Such grouping of the states according to the sign structure of the left-hand eigenvectors is, indeed, the result of a careful analysis using Perron clustering theory.⁴⁹ To minimize the effect of numerical noise, in a robust version

of Perron clustering,^{31,32,50} one can alternatively group the states on the basis of their distance in the projection onto the ψ_n^L instead of using the sign structure. We note that related methods have been used in dimensionality reduction.^{51,52}

In a variant of the above approach, one could group the states according to their splitting or commitment probability. The splitting probability, $\sigma(i)$, of a state i is the probability of reaching a certain state (or group of states) before reaching another state (or group) when starting from state i .⁵³ Transition states can be identified as states with a splitting probability near 1/2 with respect to, say, fully folded and completely unfolded states of a protein.^{54–58} For a two-state-like system, with a spectral gap after λ_2 , Berezhkovskii and Szabo⁵⁹ showed that $\sigma(i)$ is accurately approximated by the left-hand eigenvectors, shifted and scaled to the interval $[0, 1]$,

$$\sigma_n(i) = \frac{\psi_n^L(i) - \min_j \psi_n^L(j)}{\max_j \psi_n^L(j) - \min_j \psi_n^L(j)} \quad (19)$$

for $n = 2$. This relation suggests a grouping of the states in which those with $\sigma_2(i) < 1/2$ belong to one class, and those with $\sigma_2(i) \geq 1/2$, to the other. In practice, this grouping produces results very similar to those based on the sign of $\psi_2^L(i)$. The extension to multiple states involves calculating the $\sigma_n(i)$ also for $n \geq 3$.

Using the same idea, we can also calculate the exact splitting probability, ρ_i , between two states representing the two groupings. Here, those two states will be the completely unfolded state, 1, and the fully folded state, $N = 32$. The vector ρ then satisfies the linear equation

$$\rho \mathbf{K} = 0 \quad (20)$$

with “boundary conditions” $\rho_1 = 0$ and $\rho_N = 1$. Again, states would be grouped according to $\rho_i > /< 1/2$.

3. Constructing Coarse Master Equations from Simulation Trajectories

We are here interested in molecular systems in solution, such that in general, one cannot calculate the elements of the transition rate matrix easily using transition state theory.⁶⁰ Instead, we will assume that transitions have been observed in equilibrium simulations (possibly of short duration, but appropriately initialized¹⁰). However, if some of the transitions are too slow for direct sampling, one could augment the direct simulations with transition-path sampling calculations.^{61–63}

In the following, we will describe two methods to construct coarse master equations from simulation data: a simple, yet potentially less accurate lifetime-based (LB) method and a more involved maximum-likelihood (or Bayesian) propagator-based method. In both methods, we assume that we have assigned the conformations at discrete times, t_α , along the trajectory to states $s(t_\alpha) \in \{1, 2, \dots, N\}$. We note, however, that the proper assignment of states itself poses a major challenge. As will be discussed in detail below, a poor assignment manifests itself in strongly non-Markovian dynamics, in which changes in the assigned state often do not reflect actual transition events.

3.1. Lifetime-Based Estimate of the Rate Matrix. We identify transitions as times t_α at which the assigned state changes, $s(t_\alpha) \neq s(t_{\alpha-1})$. Let N_{ji} be the number of $i \rightarrow j$ transitions. Detailed balance, and microscopic time reversibility, require that for a long trajectory, $N_{ij} = N_{ji}$. To enforce detailed balance, we symmetrize the matrix of transitions: $N_{ij}^{\text{sym}} = N_{ij} + N_{ji}$. The branching probability of going from state i directly

to state j is $\Pi_{ji} = N_{ji}^{\text{sym}} / \sum_{l=1}^N N_{li}^{\text{sym}}$. T_i is the average time the system spends in state i , as estimated from the mean duration of all visits to i . We can then define the corresponding transition rate as

$$k_{ji} = \frac{\Pi_{ji}}{T_i} = \frac{N_{ji}^{\text{sym}}}{T_i \sum_{l=1}^N N_{li}^{\text{sym}}} \quad (21)$$

for $i \neq j$ and

$$k_{ii} = -T_i^{-1} = -\sum_{\substack{j=1 \\ (j \neq i)}}^N k_{ji} \quad (22)$$

These relations would be exact if the trajectory were, indeed, generated by a kinetic rate equation.

As we will show, even though the LB method is simple and easy to implement when long equilibrium trajectories are available, it is sensitive to the assignment of conformational states. With the LB approach, one needs to estimate accurate lifetimes, T_i , as well as accurate branching probabilities, Π_{ij} , both of which are difficult to obtain if transitions are not always properly identified.

3.2. Maximum-Likelihood Propagator-Based Method. An alternative method for extracting the rate matrix \mathbf{K} uses estimates of the propagators $p(j, t|i, 0)$ obtained from the simulation trajectories.¹⁰ The elements of the rate matrix are determined either by maximizing the likelihood or by Bayesian inference. Likelihood-based and Bayesian approaches proved useful also in the analysis of single-molecule experiments^{64,65} and nonlinear dynamical systems.^{66,67}

For a Markovian trajectory $s(t_\alpha) \in \{1, 2, \dots, N\}$ in the space of the N states, the probabilities of successive transitions are independent. Given a rate matrix \mathbf{K} , the likelihood of a trajectory is the product of propagators, as defined in eq 13,

$$\mathcal{L} = \prod_{t_\alpha}^{T_{\text{tot}} - \Delta t} p[s(t_\alpha + \Delta t), \Delta t | s(t_\alpha), 0] \quad (23)$$

where $\Delta t = t_{\alpha+1} - t_\alpha$ is the time interval (or lag time) used to calculate the propagator, and T_{tot} is the total simulation time. Here, we will use lag times between 1 ps and ~ 1 ns. If $N_{ji} = N_{ji}(\Delta t)$ is the number of times the trajectory is in state i at time t and state j at time $t + \Delta t$, then the likelihood can also be written as a product over states instead of times:

$$\mathcal{L} = \prod_{i=1}^N \prod_{j=1}^N [p(j, \Delta t | i, 0)]^{N_{ji}} \quad (24)$$

To find the optimal transition rates, k_{ij} , given a simulation trajectory, we maximize the likelihood function, \mathcal{L} . Alternatively, we could use Bayesian inference with an appropriate prior.¹⁰ Because of detailed balance, not all k_{ij} are independent. In particular, by using eq 4, we can write the rate matrix in terms of $N - 1$ independent equilibrium probabilities $P_{\text{eq}}(i)$ and the $N(N - 1)/2$ elements above the diagonal, or a total of $(N + 2)(N - 1)/2$ independent and positive elements. The number of parameters is further reduced if not all states are connected. Here, we will assume that transitions can occur only between neighboring states. Correspondingly, $k_{ij} = 0$ if $i - 1$ and $j - 1$ differ by more than one bit in binary notation. For $N = 2^5 =$

32 states, that reduces the number of free parameters from 527 to 111. Moreover, to improve the statistics for large lag times Δt , we will collect propagators using sliding windows. Strictly speaking, since those windows overlap, the likelihood in eq 23 would not factorize, but that will be ignored.

The procedure then is to first assign the conformations along the simulation trajectories to states. From the resulting time series in state space, $s(t_\alpha)$, we calculate the matrix N_{ji} of the number of transitions from state i to j after a fixed lag time Δt . We then find the parameters of the “optimal” rate matrix by maximizing the likelihood, \mathcal{L} . This is done by minimizing the negative logarithm of the likelihood function, $-\ln \mathcal{L}$. Specifically, we perform simulated annealing using a Metropolis Monte Carlo algorithm with parameters $\ln P_{eq}(i)$ and $\ln k_{ij}(j > i)$.¹⁰ To evaluate the likelihood for a given rate matrix, we use eq 13 with eigenvectors and eigenvalues obtained by diagonalizing the symmetrized rate matrix, eq 5, and then using eqs 7 and 9.

By comparing the results for different lag times, Δt , we can explore to what degree the dynamics is Markovian in the space of the coarse states. If it were truly Markovian, then the rate matrices for different lag times should agree within statistical noise. We expect that the eigenvalue corresponding to the slowest decaying mode will be most sensitive to non-Markovian dynamics. In particular, incorrectly identified transitions between states tend to speed up the overall relaxation. That effect is most pronounced for short lag times, suggesting that the time scale of the slowest relaxation will increase with the lag time if the dynamics is not strictly Markovian in the state space used. We note that if the lag-time dependence is large, indicating strongly non-Markovian behavior, one can attempt to expand the state space.

We note further that here $\Pi_{ji} = N_{ji}^{\text{sym}} / \sum_{l=1}^N N_{li}^{\text{sym}}$ approximates the propagator, $\Pi_{ji} \approx p(j, \Delta t | i, 0)$. Accordingly, if one is interested primarily in the long-time dynamics, one can use powers Π^k for $k = 1, 2$, etc., to propagate by $k\Delta t$ directly:^{4,5,68} $p(j, k\Delta t | i, 0) \approx [\Pi^k]_{ji}$. We note, however, that if the dynamics is, indeed, generated by a rate matrix \mathbf{K} , then the resulting transition matrix Π should have eigenvalues $\mu_n = \exp(t\lambda_n)$, and eigenvectors identical to those of \mathbf{K} . In practice, that may not be the case. In particular, even if one uses the symmetrized \mathbf{N}^{sym} that satisfies detailed balance, the eigenvalues of the corresponding transition matrix Π can actually be negative. The reason is, in effect, that the diagonal and off-diagonal elements of \mathbf{N}^{sym} obtained as simulation data samples are not necessarily balanced. Eigenvalues that are negative with statistical significance indicate that the distributions of lifetimes T_i in the states i are nonexponential, which would suggest the presence of hidden states.

4. Molecular Dynamics Simulations

We used the GROMACS 3.3 package^{69,70} to run molecular dynamics simulations of blocked alanine pentapeptide (Ala5) with explicit solvent, using the AMBER-GSS force field⁴⁶ ported to GROMACS.⁷¹ This force field is essentially identical to the AMBER-94⁷² implementation with peptide (Φ, Ψ) torsional potentials removed to reproduce experimental helix–coil equilibria⁷³ and no scaling of 1–4 van-der-Waals interactions.⁷¹

Ala5 was capped with an ACE group ($\text{CH}_3\text{CO}-$) at the N terminus, and an NME group ($-\text{NHCH}_3$) at the C terminus.⁷² We used periodic boundary conditions and the particle mesh Ewald (PME) method^{74,75} with a real-space cutoff distance of 10 Å and a grid width smaller than 1 Å.⁷⁵ All simulations were performed in the NPT ensemble with a coupling coefficient of 5 ps.^{76,70} Two-femtosecond time steps were used in conjunction with constrained bonds of hydrogen atoms.^{77,78} Structures were

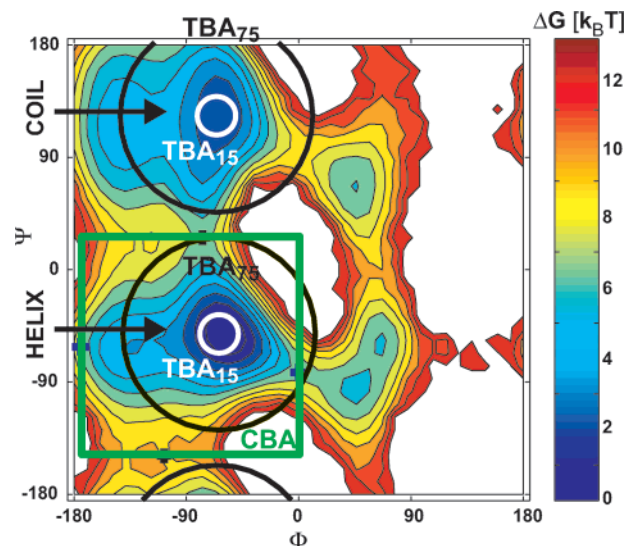


Figure 1. Ramachandran free energy surface for Ala5 from four 250-ns simulations using the Amber-GSS force field.⁴⁶ The assignments of the conformational states are illustrated by the green rectangle (CBA, purely conformation-based assignment) and by the circular boundaries (white for TBA₁₅ and black for TBA₇₅).

saved at intervals of 1 ps. The simulation box contained 1050 explicit TIP3P water molecules,⁷⁹ the total system size being 3212 atoms. The results presented in this paper were obtained by analyzing four trajectories, each of 250 ns duration at three different temperatures (250, 300, and 350 K), for a total combined simulation time of 3 μs , or 1 μs at each temperature. The trajectories were initiated from different peptide conformations: fully folded, completely unfolded, and two intermediate states (11111, 00000, 10101, and 01010 in the binary notation described below). At each temperature, it was verified that the results of the four 250-ns trajectories did not differ significantly.

4.1. Coarse-Grained Conformation Space. Here, we are not concerned with identifying the best method for coarse graining the conformational space of a molecular system. Although no general recipe is available for biomolecular systems, some guidelines have been proposed recently for the case of small peptides.^{31,33–80} Instead, we will demonstrate how one can construct useful master equations given a typical coarse-graining procedure that separates states reasonably well, but not necessarily well enough that the assumption of Markovian dynamics embodied in the master equation is fully justified.

We adopt a description of conformational states based on the (Φ, Ψ) backbone dihedral angles^{18,31} of each residue. Figure 1 shows the Ramachandran free energy profile in the (Φ, Ψ) plane averaged over the five residues.

As illustrated in Figure 1, we separate the conformations of individual amino acids into helical and nonhelical states (denoted by 1 and 0, respectively). The helical states are dominated by a minimum near $\Phi \approx \Psi \approx -50^\circ$. The nonhelical (or coil⁴⁰) states are dominated by polyproline-II- and β -strand-like conformations, with minima near $\Psi \approx 120^\circ$ and $\Phi \approx -70^\circ$ and -120° , respectively. Other conformations (in particular, the left-handed helical configuration in the upper right-hand quadrant of Figure 1) are short-lived and will be grouped together with these extended configurations into the coil state.

We denote conformations of the Ala5 peptide in a five-digit binary notation, starting with the N-terminal residue on the left. For instance, “01011” indicates that the first and third residues are in the coil state, with the second, fourth, and fifth residue in the helical state. Occasionally, we will also use a decimal notation, with states between 1 and 32 defined as their binary

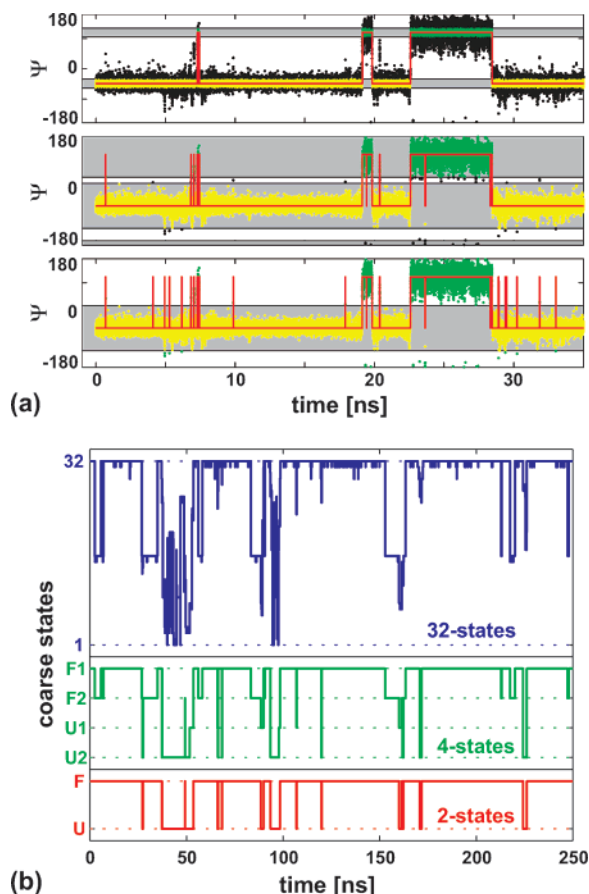


Figure 2. State assignment using CBA and TBA methods. (a) Time series (symbols) of the Ψ dihedral angle, illustrating the different conformation assignments (red lines). Pure CBA assignment (bottom panel) using Ψ ranges (light and gray shaded regions) to separate helical (yellow) and coil states (green) is contrasted to TBA that use Ψ ranges (gray shaded) for the helical and coil regions with widths of 15° (top) and 75° (middle panel). In TBA, conformations (black) located between the coil and helical regions are classified according to the neighboring regions. The assignment changes only if an actual transition is detected. (b) A 250-ns MD trajectory mapped onto 32, 4, and 2 states (top to bottom).

coding plus 1 (i.e., “01011” would then be state 12, with 1 the completely unfolded state, and 32 the fully helical state “11111”).

4.2. Assigning Peptide Conformations to States. To assign peptide conformations along the simulation trajectories to states, we will explore two different procedures. In the conventional “conformation-based assignment” (CBA), we define a rectangular region in the Ramachandran plane that covers the helical minimum (Figure 1). If the instantaneous dihedral angle pair is within that region, the state is helical (“1”); if it is outside, the state is “0”.

CBA faces the problem of fast recrossings in and out of the rectangular region. As shown by Bolhuis et al.¹⁹ and confirmed by Ma and Dinner,²⁰ the (Φ, Ψ) backbone dihedral angles alone are poor reaction coordinates for the “helix-to-coil” transition of the peptide backbone, despite being useful as coordinates in diffusion models.^{16,18} As a consequence, the actual slow transitions between helical and coil states will likely be masked by fast “recrossings” (caused by misassigned states) that do not correspond to actual transition events.

To address this problem of assigning conformations to states in the absence of a good reaction coordinate, we employ ideas from transition path sampling.^{63,81} We assume that we have a

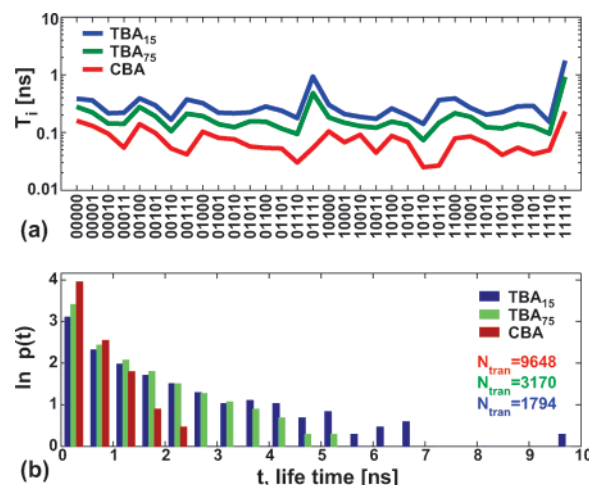


Figure 3. Lifetimes in the 32 conformational states. (a) Average lifetimes T_i (log scale) at 300 K. (b) Distribution of lifetimes without distinction of state. Results are shown for state assignments using CBA (red), TBA₁₅ (blue), and TBA₇₅ (green). The corresponding total numbers of observed transition events are also shown.

decent “order parameter” [here, (Φ, Ψ)] that allows us to assign conformations deep inside the helical and coil regions, respectively, and performs poorly only in the intermediate “transition” regions. With some confidence, we can then identify transition paths as those trajectory segments that connect without recrossing between the unambiguously helical and coil regions (i.e., they go from one region directly to the other).⁶³ Realizing that equilibration within the states is fast, it is advantageous to define the two regions relatively stringently about the respective free energy minima in order to identify proper transition paths. Even though trajectories will then frequently leave the respective regions, equilibrium excursions that do not amount to actual transitions will rapidly return, and only actual transitions will cross over from one region to the other.

In the resulting “transition-based assignment” (TBA), we define two circular region (of radius R in degrees) located around the dominant minima in the (Φ, Ψ) Ramachandran plane, Figure 1. First, transition paths are identified that connect the two circular regions. The segments between the transition paths are then assigned to the respective states (helix or coil). The first half of the transition path is assigned to the initial state; the second half, to the final state. For larger radii R , transitions become more frequent.

Figure 2a illustrates the effect of conformational assignment for a time series of the Ψ dihedral angle. In states assigned using CBA, the trajectory recrosses frequently between states with positive and negative Ψ . For TBA with a stringent condition $R = 15^\circ$, most of the fast recrossings are identified as equilibrium excursions from the minima, resulting in less frequent crossings between states. With a less stringent condition, $R = 75^\circ$, the TBA state trajectory shows slightly more frequent recrossings.

By using the TBA method to assign states, we hope to eliminate much of the fast non-Markovian dynamics associated with a poor choice of reaction coordinate. As we will show below by comparing the results for CBA and TBA with more or less stringent criteria, this is, indeed, the case.

The effect of the different methods to assign states is apparent in the average lifetimes, T_i , in each of the 32 states (Figure 3a). As expected, CBA based on the instantaneous conformation leads to short lifetimes, likely reflecting non-Markovian recrossing events. Assigning states on the basis of transition paths results in significantly longer lifetimes. For the most long-lived

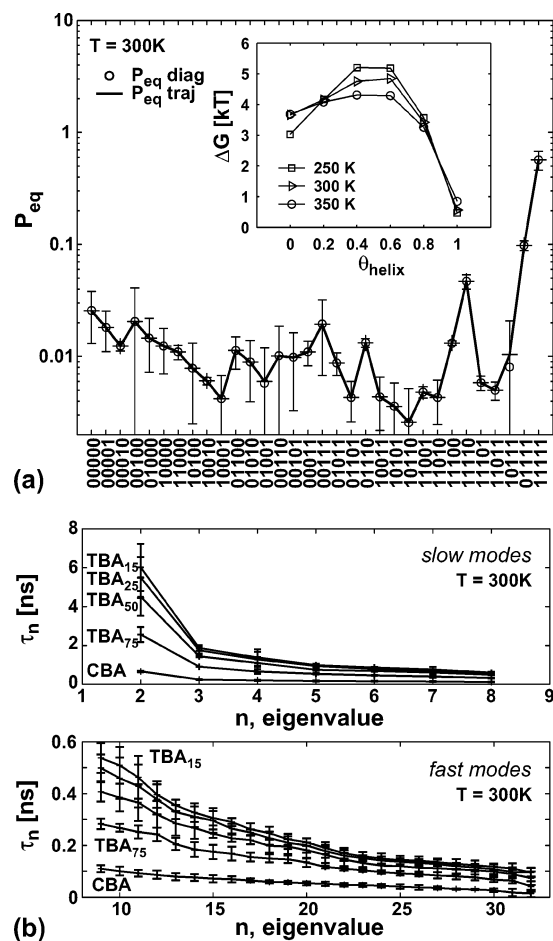


Figure 4. Populations and relaxation times from the LB master equation. (a) Equilibrium probability distribution $P_{eq}(i)$ for the 32 coarse states of Ala5 at 300 K. The inset shows the corresponding free energy vs the fraction of helical residues, illustrating the temperature dependence of the activation barrier between the 11111 (fully helical) and 00000 (completely unfolded) states. (b) Relaxation times estimated as $\tau_i = -1/\lambda_i$ by diagonalization of the LB rate matrices.

fully helical state 11111, the lifetime varies by an order of magnitude, from ~ 200 ps (CBA) to ~ 2 ns (TBA₁₅ with $R = 15^\circ$). Using a less stringent criterion (TBA₇₅ with $R = 75^\circ$) leads to a somewhat shorter lifetime (~ 1 ns for 11111). The effect of the assignment is also evident in the distributions of lifetimes (Figure 3b) averaged over all states. The CBA distributions are shifted toward short lifetimes, in comparison to the TBA₁₅ and TBA₇₅ results from which fast recrossings have been effectively eliminated.

5. Results and Discussion

5.1. Rate Matrix from Lifetime-Based Method. By using the lifetime-based method, we determined rate matrices from the four 250-ns MD trajectories of solvated Ala5 peptides at 300 K. Figure 4 shows the extracted equilibrium probabilities $P_{eq}(i)$ and relaxation times τ_n , both obtained from an eigenvalue analysis. The error bars, corresponding to one estimated standard error of the mean, were obtained from block averages.

As expected, we find that the equilibrium populations, $P_{eq}(i)$, are essentially identical for assignments of states using the CBA and TBA methods. However, the relaxation times depend strongly on how peptide conformations are assigned to states. In particular, the most slowly decaying mode has a relaxation time of < 1 ns for CBA; for TBA, that time varies

from ~ 2 to ~ 6 ns for less or more stringent assignments ($R = 75^\circ$ and 15° , respectively).

We will next use the MLPB method to construct rate matrices. This allows us to vary the time lag, in an effort to avoid problems from fast non-Markovian dynamics in the projections onto the coarse states. As we will show, for long lag times ($\Delta t \sim 1$ ns), all methods, including CBA, will converge, giving rate matrices very similar to those obtained by TBA₁₅ with lag times as short as 1 ps.

5.2. Rate Matrix from Maximum-Likelihood Propagator-Based Method. In constructing a master equation model, we are ultimately interested in predicting and understanding the slow molecular motions. If our assumption of a master equation, eq 1, were strictly valid, the resulting rate matrix would be independent of the lag time (within statistical errors). However, it seems reasonable to expect that at short times, such a model may not fully capture the fast molecular motions. The goal here is to properly extract the main characteristics of the slow molecular motions without interference from fast motions, because those are not captured by the master equation model. Therefore, we need a procedure that uses trajectory data at long time scales, where the dynamics should be sufficiently Markovian.

The MLPB method provides such a procedure by allowing us to use transition data with finite lag times. Its input is the number of times $N_{ji}(\Delta t)$ (when the system is in state j , given that it was in state i some time Δt before, independent of the states visited at intervening times). The rate matrix is inferred by maximizing the likelihood, given these data. Here, we use the fact that the propagators for the master equation can be calculated by matrix diagonalization, eq 13.

We have estimated the 32×32 rate matrices for Ala5 for lag times between 1 ps (the frequency of saving structures) to 1 ns (on the order of the time for a single dihedral angle to remain in the same state). Figure 5 shows values of the estimated equilibrium populations at 300 K for two states [(a) $P_{eq}(11111)$ and (b) $P_{eq}(11110)$] as well as the slowest (τ_2) and fastest (τ_{32}) relaxation times. The rate matrices were extracted from the four 250-ns trajectories at 300 K by using the MLPB method. For comparison, we show results for assignments of states using TBA₁₅, TBA₇₅, and CBA. For reference, we also include the results for LB rate matrices.

We find that the equilibrium populations are independent of both lag time and conformation assignment. In contrast, the relaxation times depend strongly on the lag time for CBA, somewhat less so for TBA₇₅, and relatively little for TBA₁₅. At the shortest lag time, $\Delta t = 1$ ps, the MLPB relaxation times are identical to those obtained by using the LB rate matrices for the corresponding conformation assignment. However, as the lag time increases, the slowest relaxation time τ_2 increases for CBA from ~ 0.5 ns at $\Delta t = 1$ ps to ~ 6.5 ns at $\Delta t = 1$ ns. Over the same range, τ_2 from TBA₁₅ changes from ~ 6 ns to ~ 7 ns, with statistical errors of ~ 1 ns.

Figure 6a shows the relaxation times, defined as the reciprocals $\tau_n = -1/\lambda_n$ of the eigenvalues of the rate matrix, as a function of n for different lag times and conformation assignments. For TBA₁₅, we find that the relaxation times are practically independent of lag times between 1 and 300 ps. For CBA, all relaxation times increase as the lag time increases. TBA₇₅ is intermediate, with a weak lag-time dependence. We find similar behavior for the lifetimes T_i in each of the 32 states (Figure 6b), as obtained from the rate matrix according to eq 22.

From Figures 5 and 6, we conclude that to estimate the slow molecular dynamics properly, it is important to (1) extend the analysis to sufficiently large lag times where the assumption of

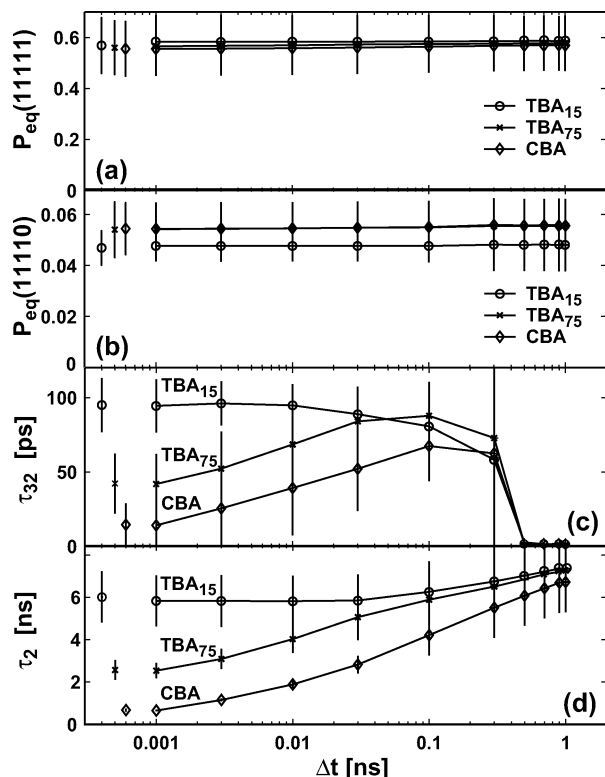


Figure 5. Populations and relaxation times from the MLPB method as a function of lag time, Δt , and for different conformational assignments (CBA, TBA₁₅, and TBA₇₅). (a) $P_{\text{eq}}(11111)$ of the most populated, fully helical state. (b) $P_{\text{eq}}(11110)$ of the state with a nonhelical C-terminal residue. (c) Fastest extracted relaxation time, $\tau_{32} = -1/\lambda_{32}$. (d) Slowest extracted relaxation time, $\tau_2 = -1/\lambda_2$ (note: $\lambda_1 = 0$). The disconnected data points (on the far left) show the corresponding results for the LB method (see Figure 4).

Markovian dynamics is justified, and (2) assign conformations to states with care. The first point effectively rules out the direct LB estimate of the rate matrix, with the exception of a conformation assignment that strongly suppresses the effects of non-Markovian dynamics (here, TBA₁₅). Assigning states on the basis of transition paths (TBA₁₅) is clearly superior to assignment on the basis of the instantaneous conformations (CBA). But remarkably, at lag times $\Delta t \approx 1$ ns, the results for all propagator-based methods converge. This convergence implies that at the nanosecond time scale, the non-Markovian character is already sufficiently weak, even for the CBA state trajectories with their poor conformation assignment.

Nevertheless, estimating the fastest relaxation processes accurately becomes increasingly difficult at large lag times Δt . Figure 5c shows that as Δt exceeds 0.1 ns, one no longer obtains a reliable estimate of τ_{32} . The reason is that this fastest relaxation is effectively at equilibrium for $\Delta t > \tau_{32}$. By using the rate matrix for $\Delta t = 10$ ps using TBA₁₅, we achieve a good tradeoff between accuracy at short and long times. In the following, we will use that rate matrix as a reference.

5.3. Validation of the Master Equation: Time Correlation Functions. As demonstrated by the results presented above, the coarse master equation extracted from given simulation trajectories depends sensitively on the way it was constructed. It is therefore of paramount importance to validate the master equation model against the simulation data. By construction, the model is nearly guaranteed to reproduce the observed equilibrium properties [here, $P_{\text{eq}}(i)$]. A more challenging validation compares the actual simulation dynamics with that predicted from the master equation.

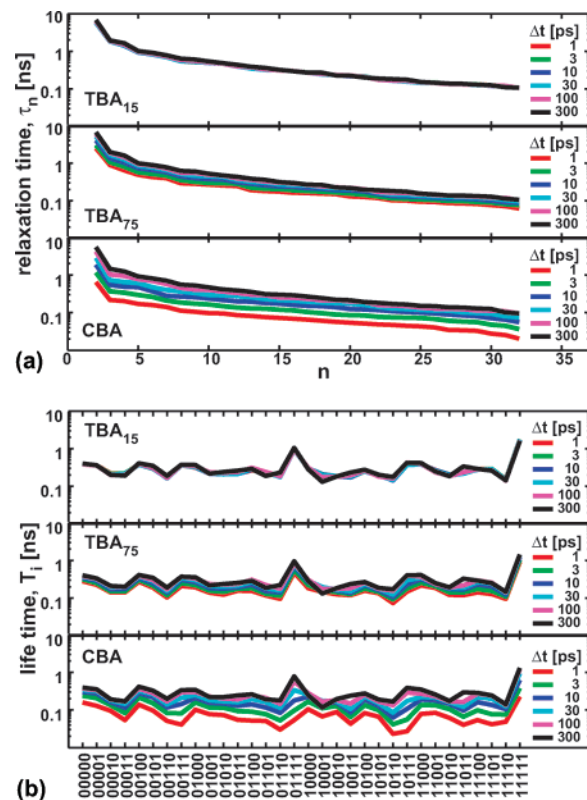


Figure 6. Relaxation times and lifetimes from the MLPB master equation. (a) Relaxation times, τ_n , of the 31 decaying modes. (b) Lifetimes $T_i = -1/k_i$ of the 32 states. Results are shown for different lag times, Δt , and conformational assignments (top to bottom: TBA₁₅, TBA₇₅, and CBA).

If the simulation trajectories are projected onto the left-hand eigenvectors, ψ_n^L , of the rate matrix, the master equation model predicts, according to eq 16, that the corresponding auto-correlation functions should decay as single exponentials with relaxation times $\tau_n = -1/\lambda_n$. The cross-correlation between projections onto two distinct modes, l and m , should be strictly zero.

We can thus use eq 16 to validate (1) the time scales of the different relaxation processes and (2) the character of the modes themselves, as captured in the weights $\psi_n^L(i)$ of state i in mode n . Normally, for any projection other than an eigenmode, the correlation function will be multiexponential with contributions from all $N = 32$ modes. Therefore, if we find single-exponential decay with the predicted relaxation times, we gain confidence not only in the temporal properties of the rate matrix but also in its “geometric” character, as reflected in its eigenmodes.

To calculate the correlation functions $C_{lm}(t)$ defined in eq 16 in practice, we use the following relation,

$$\tilde{C}_{lm}(t = n\delta t) = (\mathcal{N} - n)^{-1} \sum_{i=1}^{\mathcal{N}-n} \psi_m^L(s_{i+n}) \psi_l^L(s_i) \quad (25)$$

for the discrete time series of states $s_i = s(t_i) \in \{1, 2, \dots, 32\}$ obtained from the simulation trajectories, with $\psi_l^L(s_i)$ the s_i -th element of the vector ψ_n^L , $\delta t = t_{i+1} - t_i = 1$ ps, and \mathcal{N} the number of saved structures. Note that the lag times Δt are integer multiples of δt .

Figure 7 (top) shows the decay of the normalized auto-correlation functions $C_{nn}(t)$ for $n = 2, 3$, and 4 using the eigenvectors of the reference rate matrix (i.e., for $\Delta t = 10$ ps,

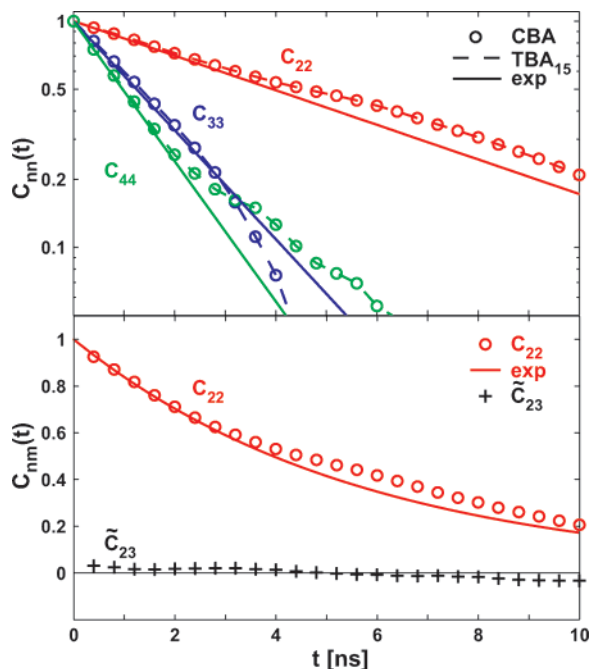


Figure 7. Mode correlation functions $C_{nm}(t)$ from the MLPB master equation and MD simulation at 300 K. The top panel compares the autocorrelation functions $C_{nn}(t)$ from the MLPB master equation (relaxation time for $\Delta t = 100$ ps lag time; Figure 6a top) for modes $n = 2$ to 4 to the simulation results obtained using CBA (circles) and TBA₁₅ (dashed lines). Note that the CBA and TBA give nearly identical correlation functions. The bottom panel compares $C_{22}(t)$ (red, circles) and the unnormalized $\tilde{C}_{23}(t)$ (black, crosses) from the CBA trajectory to the MLPB master equation predictions (lines).

TBA₁₅). Note that $C_{11}(t) \equiv 1$ is not shown. We find (1) that the correlation functions obtained for conformation assignments using CBA and TBA₁₅ are nearly identical, and (2) that they agree very well with the exponential correlation functions predicted from the reference master equation model (τ_n from Figure 6a upper panel, $\Delta t = 10$ ps). We note further that the non-Markovian “noise” in the CBA trajectories produces only a small amplitude. Also shown in Figure 7 (bottom) is the cross-correlation function $\tilde{C}_{23}(t)$, which, as predicted by eq 16, is practically zero within the noise level.

The good agreement between the correlation functions calculated using the relatively poor CBA method to assign states and the substantially better TBA₁₅ method may seem surprising at first sight. However, the $C_{nm}(t)$ correlation functions are closely related to the number correlation functions of kinetics, which can capture the correct slow population relaxation, even if the projection onto the states is relatively poor. To illustrate this point, Figure 8a schematically shows a 2D bistable free energy surface. In a projection onto x , A' states in the lower right quadrant appear to be part of B , even though they actually belong into the A meta-stable state. Similarly, B' states in the upper left quadrant appear as part of A in the projection. To estimate the effects of this poor CBA-type state assignment, in which A and B' are grouped together, as well as B and A' , we approximate the kinetics of the 2D system by the scheme in Figure 8b. If the intrawell relaxation is fast compared to the interwell relaxation and the population of misassigned states is small ($r \gg s \gg \epsilon$), then the slow phase of the normalized number correlation function for grouped states $A + B'$ and $B + A'$, respectively, has the exact relaxation rate, given by the first nonzero eigenvalue of the rate matrix, $-\lambda_2 \approx 2r\epsilon/(r + s)$. The amplitude of this slow phase is approximately $(r - s)^2/(r + s)^2$

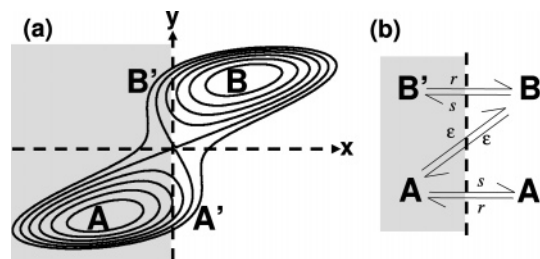


Figure 8. Projected dynamics. (a) Contour lines of a schematic bistable free energy surface. In projection onto x , A and B' states on the left ($x < 0$), and B and A' states on the right ($x > 0$) are grouped together, respectively. (b) Kinetic scheme to explore effects of state misassignment.

≈ 1 (i.e., the square of the relative difference in the populations of A and A'). With $r \gg s$ and a correspondingly small relative population of A' , the amplitude is close to one. Therefore, even for CBA with its poor projection, one approximately recovers the correct number correlation function, $\exp(\lambda_2 t)$. In contrast, propagators sampled at very short lag times will be compromised by the poor projection. In particular, for the Ala5 dynamics analyzed with the MLPB method, frequent crossings similar to those between A and B' , and B and A' are responsible for the much faster relaxations, τ_n , obtained from CBA with short lag times $\Delta t < 200$ ps (Figure 5d).

In Figure 9a, we compare the relaxation times τ_n from the reference master equation to the correlation times obtained for the TBA₁₅ projections $C_{nn}(t)$ by (a) fitting an exponential relaxation, and (b) integrating $C_{nn}(t)$ from 0 to the first (noise-induced) crossing of the zero-axis. Remarkably, we find that the relaxation times of the master equation agree with those from simulation over the entire spectrum $n = 2$ to 32. Although one could certainly have expected that the master equation accurately describes the slowest motions (τ_2), it may seem somewhat surprising that it also captures the fastest motions (τ_{32}) without “leakage” of slow motions into the predicted fast modes. However, for the Ala5 peptide studied here, the backbone dihedral angles indeed provide a fairly complete set of coordinates to describe motions on time scales beyond a few tens of picoseconds. Therefore, our set of 32 states appears to be reasonably complete at that time scale.

Nevertheless, there is some indication of weak non-Markovian dynamics, even beyond $\Delta t = 100$ ps, because the slowest relaxation time, τ_2 , gradually increases from ~ 6 to ~ 7 ns (Figure 5d). A similar value is, indeed, obtained from the exponential fit to the simulation correlation function (Figure 9a and Table 1). However, the change in the relaxation time with the lag time Δt in Figure 5d is within the statistical error, precluding a more definite analysis.

Overall, we conclude from the agreement between the actual and predicted correlation functions that the master equation model accurately captures the conformational dynamics with respect to both time scales and the character of its modes.

5.4. Temperature Dependence. To explore the temperature dependence of the folding kinetics of Ala5, we analyzed simulations at 250, 300, and 350 K. The inset of Figure 9a shows the relaxation times obtained from the reference master equations on a double logarithmic scale. Note that in supercooled solution (250 K) the conformational sampling is very slow, resulting in poor statistics. Interestingly, the spectrum approximately follows a power law, $\tau_n \propto n^{-\alpha}$, with an exponent of $\alpha \approx 1.1$, with the exception of the first eigenvalue.

Figure 9b shows that the different relaxation times τ_n obey an Arrhenius-like temperature dependence,

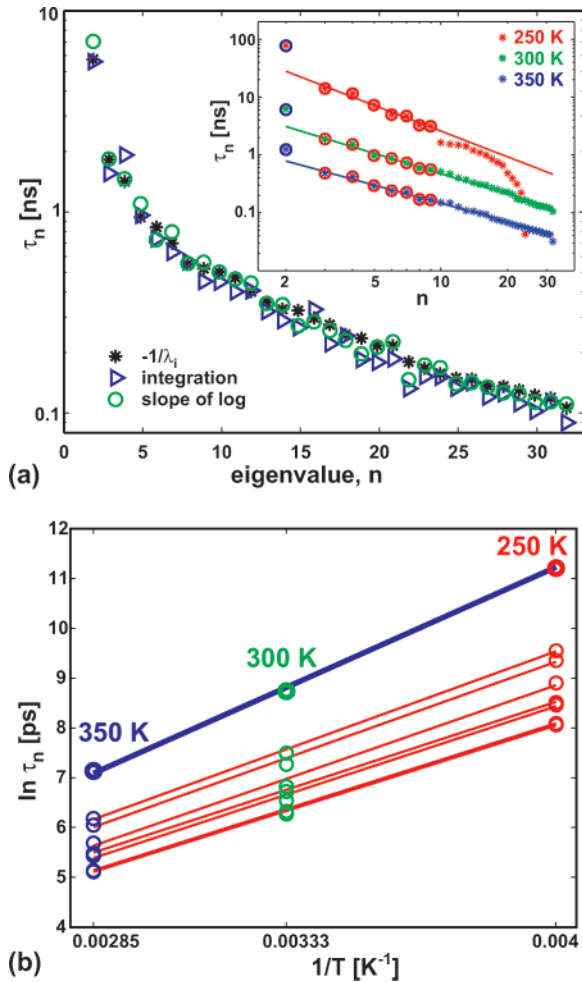


Figure 9. Relaxation times for Ala5. (a) τ_n computed using the eigenvalues of the MLPB rate matrix (black stars) and from the simulation autocorrelation functions $C_{nn}(t)$ via exponential fits (green circles) and time integration of $C_{nn}(t)$ (blue triangles). The inset shows data for $T = 250$ K (red), 300 K (green), and 350 K (blue) on a double logarithmic scale. (b) Arrhenius-like dependence of relaxation times on inverse temperature (data corresponding to the circles from the inset of part a).

$$\tau_n = A_n \exp(E_n/k_B T) \quad (26)$$

The activation energies, E_n , associated with the different exponential phases fall into different classes: $E_2 \approx 30$ kJ/mol and $E_n \approx 22$ kJ/mol for $3 \leq n \leq 9$. The larger value for E_2 can be explained by the fact that the corresponding process involves the breaking and formation of backbone hydrogen bonds, in addition to changing the backbone dihedral angles.

5.5. Conformational Clustering: Reduced Representation of the Master Equation. The presence of a significant gap in the relaxation spectrum (Figure 9a) after the first eigenvalue suggests that the system can be represented approximately by two states alone: folded (F) and unfolded (U). To assign each of the 32 microstates to U or F, we use (1) the sign of the elements of the left-hand eigenvector $\psi_2^L(i) = \phi_2(i)/\phi_1(i)$, (2) $\sigma_2(i) > /< 0.5$ according to eq 19, and (3) $\rho_i > /< 0.5$ according to eq 20 with $\rho_i = 0$ for $i = 1$ (“00000”) and $\rho_i = 1$ for $i = 32$ (“11111”).

Figure 10a shows the resulting assignments of each of the 32 states. In particular, we find that states 11111 and 11110 consistently belong to the folded state F. In contrast, 01111 and 01110 with a nonhelical residue at the N terminus belong to the folded state according to $\sigma_2(i)$ and ρ_i but not according to

TABLE 1: Relaxation Times, τ_n , for the Full 32-State System and for the 2- and 4-State Reduced Representations^a

n	a_n	τ_n [ps]
32-State System		
2	0.964	7030
3	0.997	1990
4	0.982	1490
5	0.967	1170
...		
32	0.997	104
2-State Projection		
$s(t)$ from ϕ_2/ϕ_1		
2	0.862	6380
$s(t)$ from $\sigma_2(i)$		
2	0.929	6280
$s(t)$ from ρ_i		
2	0.764	5560
4-State Projection		
2	0.929	7110
3	0.996	1770
4	0.978	1360

^a The relaxation times, τ_n , were obtained from single-exponential fits [$a_n \exp(-t/\tau_n)$] to the normalized autocorrelation functions $C_{nn}(t)$, excluding an initial fast relaxation from the fit. The $C_{nn}(t)$ were obtained from the simulation trajectories by projecting them onto the ψ_n^L according to eq 25. For the two-state system, the coarse trajectories $s(t)$ were obtained by clustering states using the sign of $\phi_2(i)/\phi_1(i)$ or the splitting probabilities $\sigma_2(i)$ and ρ_i , as indicated. The four-state clustering was performed as illustrated in Figure 10.

the sign structure of $\psi_2^L(i) = \phi_2(i)/\phi_1(i)$. Figure 2b shows one of the resulting two-state trajectories.

This and other ambiguities raise the question concerning how useful the groupings into folded and unfolded states are. To address that question, we calculate the normalized number correlation function $c(t) = \langle \delta n(t) \delta n(0) \rangle / \langle \delta n^2 \rangle$ where $\delta n(t) = n(t) - \langle n(t) \rangle$, and $n(t)$ is 1 if the system is in one of the folded states, and 0, otherwise. As illustrated in Figure 8 and discussed above, the number correlation function can capture the correct slow population relaxation, even if the projection onto the states is poor. We can therefore use $c(t)$ as a reference. Specifically, we fit the $c(t)$ calculated from the MD data to a single exponential (beyond ~ 1 ns). To assess the quality of the grouping, we compare the resulting relaxation times to that obtained for projecting onto the full 32-state system (~ 7 ns; Figure 9).

Table 1 lists the amplitudes and relaxation times of the single-exponential fits to the number correlation functions for the three different two-state groupings. We find that the two clusterings according to $\phi_2(i)/\phi_1(i)$ and $\sigma_2(i) > /< 0.5$ produce consistent results, with relaxation times of ~ 6.3 ns, and amplitudes of ~ 0.9 in the slow phase, as compared to a relaxation time of 7 ns and amplitude of 0.96 for the 32-state trajectory. In contrast, the grouping according to the “exact” splitting probabilities ρ_i produces a worse result, with a relaxation time of only 5.5 ns and an amplitude of 0.76. Moreover, when we actually fit a two-state model to the simulation data using the MLPB approach and a lag time of 100 ps, we obtain a relaxation time of only 3.8 ns (Figure 11). We conclude from these discrepancies that the two-state models built using the $\phi_2(i)/\phi_1(i)$ and $\sigma_2(i) > /< 0.5$ clusterings give an adequate, although not perfect, description of the kinetics.

To improve the reduced model, we expand the state space to four states. The reason to skip the three-state model is that $\tau_3 \approx \tau_4$ according to Figure 9a. To group the states, we project the 32 states onto $\psi_2^L(i) = \phi_2(i)/\phi_1(i)$, $\psi_3^L(i) = \phi_3(i)/\phi_1(i)$, and

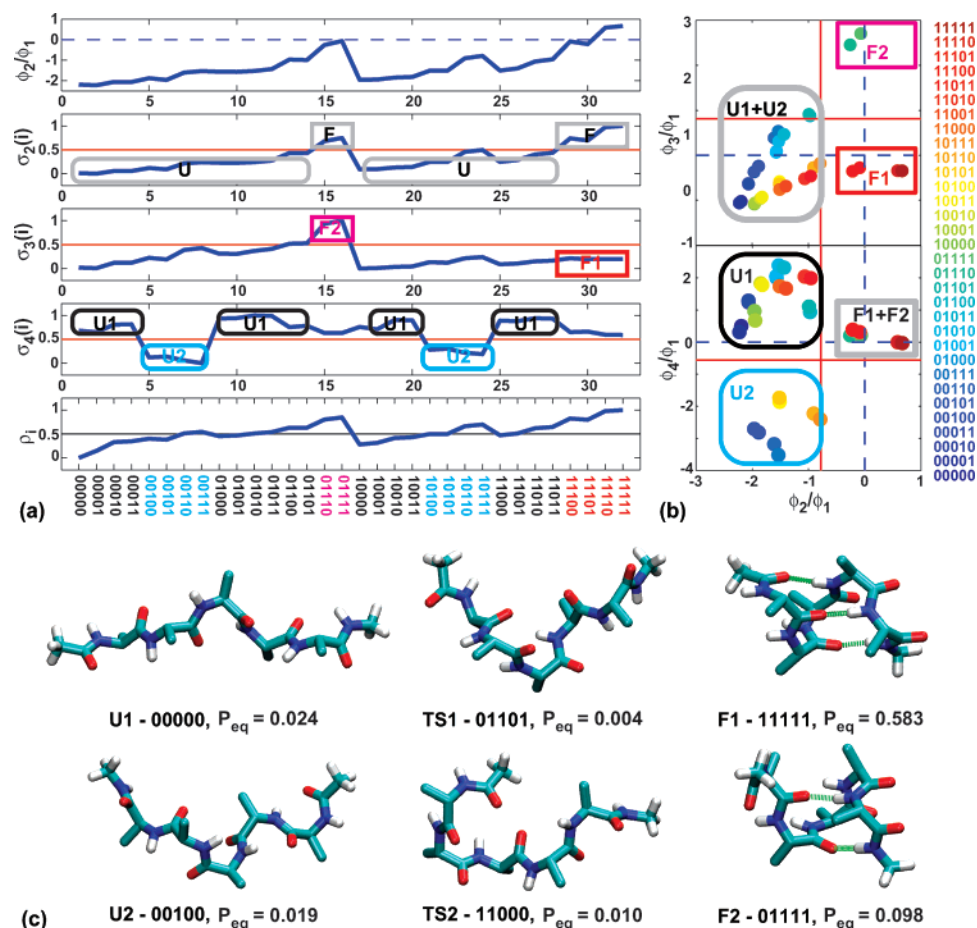


Figure 10. Coarse graining of conformational space. (a) Eigenvector-based clustering of conformational states using the sign of $\phi_2(i)/\phi_1(i)$ (top), shifted and rescaled $\sigma_n(i)$ (middle panels, $n = 2, 3, 4$), and splitting probability ρ_i (bottom, see eq 20). (b) Clustering of states using ϕ_3/ϕ_1 (top) and ϕ_4/ϕ_1 (bottom) plotted vs ϕ_2/ϕ_1 . The solid horizontal and vertical red lines indicate $\sigma_n = 0.5$ used in the four-state clustering. Clustering according to the sign structure would use the blue dashed lines, instead. (c) Representative molecular structures of folded (F1 and F2) and unfolded states (U1 and U2). $(i, i + 4)$ hydrogen bonds are indicated in green. Transition states (TS1 and TS2) were selected from states with $\sigma_2(i) \approx 0.5$.

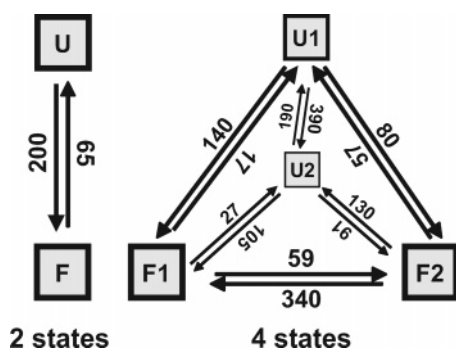


Figure 11. Transition rates (in units of μs^{-1}) for the 2-state (left) and 4-state reduced representations obtained by eigenvector-based clustering of the 32 conformational states of Ala5 at $T = 300$ K.

$\psi_4^L(i) = \phi_4(i)/\phi_1(i)$. As shown in Figure 10a and b, ψ_2^L separates the folded from the unfolded states and corresponds to the slowest relaxation (7 ns). ψ_3^L splits the folded state into two groups, but leaves the unfolded state intact, and ψ_4^L splits the unfolded state into two groups without affecting the folded state. However, instead of grouping by the sign structure of the $\psi_n^L(i)$ (dashed zero axis in Figure 10b), we use the shifted and rescaled $\sigma_2(i)$, $\sigma_3(i)$, and $\sigma_4(i)$ to group the states (solid red lines in Figure 10b). We end up with four states: two folded states, F1 and F2, and two unfolded states, U1 and U2.

The configurations belonging to each of the four states are indicated by color in Figure 10a: F1 (purple), F2 (red), U1

(black), and U2 (blue). We find that the folded substates F1 and F2 jointly contain all states with at least three consecutive helical dihedral angles (“111”) within the four N-terminal residues and, thus, all structures with at least one $(i, i + 4)$ α -helical hydrogen bond in that segment. The difference between F1 and F2 is that in F1, the N-terminal residue is in a coil state, whereas in F2, it is helical. (We note that this indicates slow relaxation at the N terminus and fast relaxation at the C terminus, consistent with earlier findings.^{45,82}) Figure 10c shows representative molecular structures of folded (F1 and F2) and unfolded (U1 and U2) conformations. Hydrogen bonds are shown in green. Also shown are representative “transition states” (TS1 and TS2) with splitting probabilities close to 0.5. Figure 2b shows one of the trajectories projected onto the four states.

To validate the four-state model, we could calculate the number correlation functions for each of the four states. However, those will in general be multiexponential. Instead, we construct a 4×4 rate matrix using the MLPB procedure for the TBA₁₅ trajectory projected onto the four states. This rate matrix provides us with new, four-element left-hand eigenvectors onto which we can project the simulation trajectories. Ideally, the autocorrelation functions calculated according to eqs 16 and 25 should be single-exponential.

Table 1 lists the amplitudes and relaxation times for the three decaying correlation functions obtained by exponential fits. If the four-state model captured the slow relaxations properly, the time constants would be the same as those corresponding to

the first three nonzero eigenvalues of the 32-state model, and the amplitudes should be one. Indeed, we find excellent agreement. In particular, the slowest relaxation has a time constant of 7.1 ns, as compared to 7.0 ns for the 32-state system, and the amplitude is 0.93. We conclude that the projections onto the left-hand eigenvectors provide excellent (though not entirely unambiguous) criteria to group states into clusters.

Figure 11 shows the kinetic rate coefficients of the two-state and four-state models, both obtained from MLPB analysis. Interestingly, the four-state model is fully connected. However, the relaxations between U1 and U2 and between F1 and F2 are, indeed, faster than between U and F states, consistent with the ordering of the eigenvalues associated with the different relaxation processes.

In summary, we found that a two-state representation with a folded and an unfolded state provides a good approximation to the full dynamics. A four-state description, with two folded and two unfolded states, recovers accurately the first three relaxation processes.

6. Conclusions

We showed that a 32-state master equation could accurately describe the conformational dynamics of blocked Ala5, a short helix-forming peptide. Our detailed analysis demonstrates that accurate master equations are obtained (1) if conformational states are assigned by using transition paths (TBA) rather than instantaneous conformations (CBA) and (2) if a propagator-based method is used with long lag times (here, 10 ps to 1 ns). To identify transition paths in the TBA method, using dihedral angles is a reasonable choice, without the need for high-quality reaction coordinates.^{63,81} To extract rates, propagator-based methods are superior to direct, lifetime-based approaches because they suppress the effects of fast non-Markovian dynamics. Accordingly, even for trajectories with poorly assigned states, the propagator-based (MLPB) method leads to systematically better estimates of the intrinsic transition rates.

Here, we used long equilibrium simulations (covering $3 \times 1 \mu\text{s}$) to parametrize the master equation. However, as we showed, transition matrices for lag times as short as 1 ps can be used to construct accurate master equation models, as long as transition-path methods are used to assign states. Accordingly, one can use either properly initialized short MD runs¹⁰ or replica-exchange molecular dynamics runs^{73,83} with swapping intervals >1 ps to obtain the input transition matrices. In the case of replica-exchange simulations, states could be assigned using TBA by following the trajectories in temperature space.⁸⁴

As an important aspect, we showed that master equation models can be explicitly validated by comparing predicted correlation functions to those obtained directly from simulation. Specifically, we projected the simulation trajectories onto the left-hand eigenvectors of the rate matrix and found that the resulting auto-correlation functions have single-exponential decays with relaxation times as predicted from the eigenvalues of the rate matrix. We also showed that the cross-correlations between the projections vanish, as predicted. The excellent agreement of the correlation functions shows that the master equation captures not only the relaxation times but also the character of the different relaxation modes.

Gaps in the eigenvalue spectrum of the master equation also suggest further reductions from 32 to 2 and 4 states, respectively. This coarse graining is achieved by grouping states together into clusters according to their projection onto the eigenvectors of the slowest-decaying modes. We show that we can reduce the system roughly to two states, folded and unfolded. The

folded state is found to contain all structures with at least one ($i, i + 4$)-type α -helical hydrogen bond within the four N-terminal amino acids. However, the number correlation function for the two-state projection decays substantially faster than the slowest relaxation process seen in the actual simulation trajectories. A more faithful representation of the full dynamics is obtained by using four states, two each for the unfolded and folded ensembles. The slow relaxation in the folded state, with a relaxation time of ~ 2 ns, is associated with the transition of the N-terminal amino acid between helix and coil states. In summary, we found that the construction of master equations using propagator-based methods not only allowed us to explore the long-time dynamics, but also provides detailed insights into the mechanisms of the folding dynamics of a peptide.

Acknowledgment. We thank Dr. Attila Szabo and Dr. Alexander Berezhkovskii for many helpful and stimulating discussions. This research utilized the high-performance computational capabilities of the Biowulf Linux cluster at the NIH (<http://biowulf.nih.gov>), and it was supported by the Intramural Research Program of the NIDDK, NIH.

References and Notes

- (1) Mohanty, D.; Elber, R.; Thirumalai, D.; Beglov, D.; Roux, B. *J. Mol. Biol.* **1997**, *272*, 423–442.
- (2) Schütte, C.; Fischer, A.; Huisinga, W.; Deuffhard, P. *J. Comput. Phys.* **1999**, *151*, 146–168.
- (3) Huisinga, W.; Schütte, C.; Stuart, A. M. *Commun. Pure Appl. Math.* **2003**, *56*, 234–269.
- (4) Swope, W. C.; Pitera, J. W.; Suits, F. *J. Phys. Chem. B* **2004**, *108*, 6571–6581.
- (5) Swope, W. C.; Pitera, J. W.; Suits, F.; Pitman, M.; Eleftheriou, M.; Fitch, B. G.; Germain, R. S.; Rayshubski, A.; Ward, T. J. C.; Zhestkov, Y.; Zhou, R. *J. Phys. Chem. B* **2004**, *108*, 6582–6594.
- (6) Levy, Y.; Jortner, J.; Berry, R. S. *Phys. Chem. Chem. Phys.* **2002**, *4*, 5052–5058.
- (7) Chekmarev, D. S.; Ishida, T.; Levy, R. M. *J. Phys. Chem. B* **2004**, *108*, 19487–19495.
- (8) de Groot, B. L.; Daura, X.; Mark, A. E.; Grubmüller, H. *J. Mol. Biol.* **2001**, *309*, 299–313.
- (9) Becker, O. M.; Karplus, M. *J. Chem. Phys.* **1997**, *106*, 1495–1517.
- (10) Sriraman, S.; Kevrekidis, I. G.; Hummer, G. *J. Phys. Chem. B* **2005**, *109*, 6479–6484.
- (11) Zwanzig, R. *J. Stat. Phys.* **1983**, *30*, 255–262.
- (12) Zwanzig, R.; Szabo, A.; Bagchi, B. *Proc. Natl. Acad. Sci. U.S.A.* **1992**, *89*, 20–22.
- (13) Bryngelson, J. D.; Wolynes, P. G. *J. Phys. Chem.* **1989**, *93*, 6902–6915.
- (14) Schonbrun, J.; Dill, K. *Proc. Natl. Acad. Sci. U.S.A.* **2003**, *100*, 12678–12682.
- (15) Bicout, D. J.; Szabo, A. *J. Chem. Phys.* **1998**, *109*, 2325–2338.
- (16) Hummer, G. *New J. Phys.* **2005**, *7*, 34.
- (17) Best, R. B.; Hummer, G. *Phys. Rev. Lett.* **2006**, *96*, 228104.
- (18) Hummer, G.; Kevrekidis, I. G. *J. Chem. Phys.* **2003**, *118*, 10762–10773.
- (19) Bolhuis, P. G.; Dellago, C.; Chandler, D. *Proc. Natl. Acad. Sci. U.S.A.* **2000**, *97*, 5877–5882.
- (20) Ma, A.; Dinner, A. R. *J. Phys. Chem. B* **2005**, *109*, 6769–6779.
- (21) Hummer, G. *J. Chem. Phys.* **2004**, *120*, 516.
- (22) Rhee, Y. M.; Pande, V. S. *J. Phys. Chem. B* **2005**, *109*, 6780–6786.
- (23) Ren, W.; Vanden-Eijnden, E.; Maragakis, P.; E, W. *J. Chem. Phys.* **2005**, *123*, 134109.
- (24) Elmer, S. P.; Park, S.; Pande, V. S. *J. Chem. Phys.* **2005**, *123*, 114902.
- (25) Elmer, S. P.; Park, S.; Pande, V. S. *J. Chem. Phys.* **2005**, *123*, 114903.
- (26) Snow, C. D.; Sorin, E. J.; Rhee, Y. M.; Pande, V. S. *Annu. Rev. Biophys. Biomol. Struct.* **2005**, *34*, 43–69.
- (27) Singhal, N.; Pande, V. S. *J. Chem. Phys.* **2005**, *123*, 204909.
- (28) Singhal, N.; Snow, C. D.; Pande, V. S. *J. Chem. Phys.* **2004**, *121*, 415.
- (29) van der Spoel, D.; Seibert, M. M. *Phys. Rev. Lett.* **2006**, *96*, 238102.
- (30) Chodera, J. D.; Swope, W. C.; Pitera, J. W.; Dill, K. A. *Multiscale Model. Sim.* **2006**, *5*, 1214–1226.

- (31) Noe, F.; Horenko, I.; Schütte, C.; Smith, J. C. *J. Chem. Phys.* **2007**, *126*, 155102.
- (32) Kube, S.; Weber, M. *J. Chem. Phys.* **2007**, *126*, 024103.
- (33) Chodera, J. D.; Singhal, N.; Pande, V. S.; Dill, K. A.; Swope, W. C. *J. Chem. Phys.* **2007**, *126*, 155101.
- (34) Poland, D. C.; Scheraga, H. A. *Theory of the helix-coil transition*; Academic Press: New York, 1970.
- (35) Scheraga, H. A.; Vila, J. A.; Ripoll, D. R. *Biophys. Chem.* **2002**, *101*, 255–265.
- (36) Graf, J.; Nguyen, P. H.; Stock, G.; Schwalbe, H. *J. Am. Chem. Soc.* **2007**, *129*, 1179–1189.
- (37) Wang, T.; Du, D.; Gai, F. *Chem. Phys. Lett.* **2003**, *370*, 842–848.
- (38) Thompson, P. A.; Eaton, W. A.; Hofrichter, J. *Biochemistry* **1997**, *36*, 9200–9210.
- (39) Doshi, U.; Muñoz, V. *Chem. Phys.* **2004**, *307*, 129–136.
- (40) Buchete, N. V.; Straub, J. E. *J. Phys. Chem. B* **2001**, *105*, 6684–6697.
- (41) van Giessen, A. E.; Straub, J. E. *J. Chem. Phys.* **2005**, *122*, 024904.
- (42) van Giessen, A. E.; Straub, J. E. *J. Chem. Theory Comput.* **2006**, *2*, 674–684.
- (43) Daidone, I.; D'Abramo, M.; Di Nola, A.; Amadei, A. *J. Am. Chem. Soc.* **2005**, *127*, 14825–14832.
- (44) Hummer, G.; García, A. E.; Garde, S. *Phys. Rev. Lett.* **2000**, *85*, 2637–2640.
- (45) Hummer, G.; García, A. E.; Garde, S. *Proteins* **2001**, *42*, 77–84.
- (46) Nymeyer, H.; García, A. E. *Proc. Natl. Acad. Sci. U.S.A.* **2003**, *100*, 13934–13939.
- (47) Margulis, C. J.; Stern, H. A.; Berne, B. J. *J. Phys. Chem. B* **2002**, *106*, 10748–10752.
- (48) Bicout, D. J.; Szabo, A. *Protein Sci.* **2000**, *9*, 452–465.
- (49) Deuffhard, P.; Huisinga, W.; Fischer, A.; Schütte, C. *Linear Algebra Appl.* **2000**, *315*, 39–59.
- (50) Deuffhard, P.; Weber, M. *Linear Algebra Appl.* **2005**, *398*, 161–184.
- (51) Belkin, M.; Niyogi, P. *Neural Comput.* **2003**, *15*, 1373–1396.
- (52) Coifman, R. R.; Lafon, S.; Lee, A. B.; Maggioni, M.; Nadler, B.; Warner, F.; Zucker, S. *Proc. Natl. Acad. Sci. U.S.A.* **2004**, *102*, 7426–7431.
- (53) Onsager, L. *Phys. Rev.* **1938**, *54*, 554–557.
- (54) Du, R.; Pande, V. S.; Grosberg, A. Y.; Tanaka, T.; Shakhnovich, E. S. *J. Chem. Phys.* **1998**, *108*, 334–350.
- (55) Geissler, P. L.; Dellago, C.; Chandler, D. *J. Phys. Chem. B* **1999**, *103*, 3706–3710.
- (56) Best, R. B.; Hummer, G. *Proc. Natl. Acad. Sci. U.S.A.* **2005**, *102*, 6732–6737.
- (57) Snow, C. D.; Rhee, Y. M.; Pande, V. S. *Biophys. J.* **2006**, *91*, 14–24.
- (58) Berezhkovskii, A.; Szabo, A. *J. Chem. Phys.* **2006**, *125*, 104902.
- (59) Berezhkovskii, A.; Szabo, A. *J. Chem. Phys.* **2004**, *122*, 014503.
- (60) Wales, D. J. *Mol. Phys.* **2002**, *100*, 3285–3305.
- (61) Dellago, C.; Bolhuis, P. G.; Chandler, D. *J. Chem. Phys.* **1999**, *110*, 6617–6625.
- (62) van Erp, T. S.; Moroni, D.; Bolhuis, P. G. *J. Chem. Phys.* **2003**, *118*, 7762–7774.
- (63) Hummer, G. *J. Chem. Phys.* **2004**, *120*, 516–523.
- (64) Andrec, M.; Levy, R. M.; Talaga, D. S. *J. Phys. Chem. A* **2003**, *107*, 7454–7464.
- (65) Kou, S. C.; Xie, X. S.; Liu, J. S. *Appl. Stat.* **2005**, *54*, 1–28.
- (66) McSharry, P. E.; Smith, L. A. *Phys. Rev. Lett.* **1999**, *83*, 4285–4288.
- (67) Meyer, R.; Christensen, N. *Phys. Rev. E: Stat. Phys., Plasmas, Fluids, Relat. Interdiscip. Top.* **2000**, *62*, 3535–3542.
- (68) Hinrichs, N. S.; Pande, V. S. *J. Chem. Phys.* **2007**, *126*, 244101.
- (69) van der Spoel, D.; Lindahl, E.; Hess, B.; Groenhof, G.; Mark, A. E.; Berendsen, H. J. C. *J. Comput. Chem.* **2005**, *26*, 1701–1718.
- (70) Lindahl, E.; Hess, B.; van der Spoel, D. *J. Mol. Model.* **2001**, *7*, 306–317.
- (71) Sorin, E. J.; Pande, V. S. *Biophys. J.* **2005**, *88*, 2472–2493.
- (72) Cornell, W. D.; Cieplak, P.; Bayly, C. I.; Gould, I. R.; Merz, K. M.; Ferguson, D. M.; Spellmeyer, D. C.; Fox, T.; Caldwell, J. W.; Kollman, P. A. *J. Am. Chem. Soc.* **1995**, *117*, 5179–5197.
- (73) García, A. E.; Sanbonmatsu, K. Y. *Proc. Natl. Acad. Sci. U.S.A.* **2002**, *99*, 2782–2787.
- (74) Darden, T.; York, D.; Pedersen, L. *J. Chem. Phys.* **1993**, *98*, 10089–10092.
- (75) Essmann, U.; Perera, L.; Berkowitz, M. L.; Darden, T.; Lee, H.; Pedersen, L. G. *J. Chem. Phys.* **1995**, *103*, 8577.
- (76) Berendsen, H. J. C.; Postma, J. P. M.; van Gunsteren, W. F.; DiNola, A.; Haak, J. R. *J. Chem. Phys.* **1984**, *81*, 3684–3690.
- (77) Miyamoto, S.; Kollman, P. A. *J. Comput. Chem.* **1992**, *13*, 952–962.
- (78) Hess, B.; Bekker, H.; Berendsen, H. J. C.; Fraaije, J. G. E. M. *J. Comput. Chem.* **1997**, *18*, 1463–1472.
- (79) Jorgensen, W. L.; Chandrasekhar, J.; Madura, J. D.; Impey, R. W.; Klein, M. L. *J. Chem. Phys.* **1983**, *79*, 926–935.
- (80) Jayachandran, G.; Vishal, V.; Pande, V. S. *J. Chem. Phys.* **2006**, *124*, 164902.
- (81) Bolhuis, P. G.; Chandler, D.; Dellago, C.; Geissler, P. L. *Annu. Rev. Phys. Chem.* **2002**, *53*, 291–318.
- (82) Tobias, D. J.; Brooks, C. L. *Biochemistry* **1991**, *30*, 6059–6070.
- (83) Andrec, M.; Felts, A. K.; Gallicchio, E.; Levy, R. M. *Proc. Natl. Acad. Sci. U.S.A.* **2005**, *102*, 6801–6806.
- (84) Buchete, N.-V.; Hummer, G. Submitted, [<http://arxiv.org/abs/0710.5533>].